

Detection of Variabilities and Trends in the Tropical and South Atlantic Ocean Using Hydrodynamic Numerical Modeling

Joseph Harari^{1*}, Nair Emmanuela da Silveira Pereira² and Ricardo de Camargo³

¹Oceanographic Institute, University of Sao Paulo, Sao Paulo, Brazil

²Program of Ocean Engineering (Peno)/COPPE, Federal University of Rio de Janeiro (UFRJ), Brazil

³Institute of Astronomy, Geophysics and Atmospheric Sciences, University of Sao Paulo, Sao Paulo, Brazil

*Corresponding author: Joseph Harari, Oceanographic Institute, University of Sao Paulo, Sao Paulo, Brazil, Tel: 55-11-30916576/55-11-974180918; E-mail: joharari@usp.br

Rec date: Apr 06, 2016; Acc date: May 17, 2016; Pub date: May 24, 2016

Copyright: © 2016 Harari J, et al. This is an open-access article distributed under the terms of the Creative Commons Attribution License, which permits unrestricted use, distribution, and reproduction in any medium, provided the original author and source are credited.

Abstract

This project aims to detect variabilities and trends in outputs of a three dimensional hydrodynamical numerical model based on a version of the Princeton Ocean Model (POM), covering the region between 85°S-30°N and 70°W-25°E, with 0.5° x 0.5° resolution. Surface data of temperature and salinity, from Climate Forecast System Reanalysis (CFSR), together with meteorological data of winds and surface fluxes, generated by reanalyses of NCEP/NCAR global model, were used as model forcings. The temperature-salinity data, meteorological data and model results cover the period from 1980 to 2009 (30 years). The model was validated through comparisons with outputs of oceanic buoy data from the PIRATA project (for the period 1997-2009) and satellite measurements by MODIS sensor (for the period 2003-2009). Model results and sea surface temperature data from PIRATA display strong correlations, both in the annual and higher frequencies signals. Even filtering the annual and semi-annual signals in the surface temperature series, model results and buoy data have mean value of linear correlation 0.59 ± 0.07 and mean value of Wilmott parameter 0.57 ± 0.15 . The model results showed a mean difference of temperature to PIRATA series of $0.44 \pm 0.26^\circ\text{C}$, denoting a slight underestimation of the temperatures computed by the model. The comparison of temperature profiles from the model to the PIRATA buoys shows that the model can be considered valid to surface data, but need some improvement in depth. Harmonic and statistical analyzes of selected points, applied to meteorological parameters, sea surface elevation, temperature, salinity and currents provide information on the variabilities and trends in the Tropical and South Atlantic Ocean. As an example, an extremely high trend of surface temperature was found in the Equatorial region and in the latitude belt of 40°S, for the period 2003-2009, reaching above $+0.2^\circ\text{C}/\text{year}$. In this period, a trend of -0.01 m/s/year was computed for the equatorial surface currents, surrounded by trends of $+0.01$ m/s/year off the African coast, at about 3°N and 3°S. However, an analysis in a longer period of time would be needed for more conclusive statements. Analyses of the distributions of the standard deviations show that seasonality is not always the main factor responsible for most of the standard deviation, such as for the intensity of the currents in the equatorial region.

Keywords: Variabilities and trends; Tropical and South Atlantic Ocean; Numerical modeling; Buoys data

Introduction

Numerical modeling has been increasingly used in Oceanography as an important method for analysis, simulations and predictions of spatial-temporal distribution of hydrodynamic and thermodynamic parameters. The ocean models are an approximation of physical theories in which simplifications are often deliberately introduced [1]. As an example, the Princeton Ocean Model (POM), created in 1977 to be a model for predicting hydrodynamics in coastal and estuarine areas, by Blumberg and Mellor [2]. The POM is based on sigma vertical coordinates, which considers vertical levels as percentages of total depth, allowing the maintenance of high vertical resolution in shallow regions. The use of this type of vertical coordinate is suitable for regions with high topographic variation, because it allows an accurate representation of their hydrodynamics. Examples include studies on mesoscale simulations, as the pioneer one of Blumberg and Mellor for coastal regions, but also for large-scale models, as those of Ezer and Mellor [3-5] for the North Atlantic.

For the correct applicability of a model, it is necessary to validate it by comparing its results with results from other measurements or models. Validation is part of a process that aims to indicate the possible existence of errors in a model, so that it can be improved, in order to increase the level of confidence in its ability to reproduce events of interest [6,7]. There are several sources of errors in model simulations, most of them related to the specification of boundary conditions [5] or initial conditions and data assimilation techniques [8].

A good option for data validation of hydrodynamic modeling of the tropical Atlantic is the Operational Programme "Pilot Research Moored Array in the Tropical Atlantic" (PIRATA), a multinational effort of Brazil, France and the United States, designed to obtain meteorological and oceanographic data from moored buoys in this area. This program was initiated in 1997 and is maintained permanently since then [9].

Thus, the aim of this work is to calibrate and validate the implementation of the POM in the Tropical and South Atlantic [10-12], based on data from anchored buoys PIRATA and remote sensing data (MODIS). After that, trends and variabilities of the model results were analyzed, for the period 2003-2009.

Study area

The area under study in this project is the Tropical and South Atlantic Ocean (Figure 1) that has a complex system of surface currents characterized by the presence of an anticyclonic rotation forced mainly by wind [13,14], with strong associated features. As an example, we have the Retroflexion of the Agulhas Current and the confluence of the Brazil and Malvinas Currents along the South America continental shelf, forming a complex pattern of meanders and eddies [15]. Tropical and South Atlantic has a large seasonal variability of surface currents, upwelling regions, temperature and salinity [16], which can be related to variations in atmospheric forcings that also exhibit significant seasonal character [17]. Such variabilities may induce variations of biological responses.

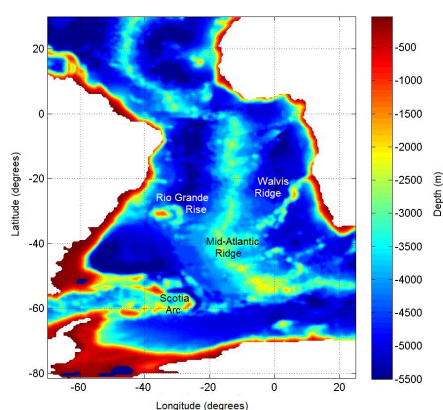


Figure 1: Study area-Tropical and South Atlantic Ocean and its bathymetry.

Data and Methods

The model

The hydrodynamic model implemented in this study is a version of POM written by Mellor and Blumberg [2], described and optimized by

Harari et al. [18]. This implementation uses high-resolution grids for the Tropical and South Atlantic and Brazilian Continental Shelf, considering simulations of the circulation generated by tides, winds and density variations. This version has been used for scientific and operational purposes, allowing the reproduction of the hydrodynamics in this area and any subdomain, through nested grids, especially in coastal and continental shelf [11,18].

POM is a three-dimensional model that considers free surface and solves a set of three-dimensional nonlinear primitive equations of motion, discretized by the finite difference method and considering modes separation. It is through this modes separation that volume transport (external mode) and velocity shear in the vertical (internal modes) are solved separately, saving computation time.

The complete hydrodynamic equations are written in the flux form, considering Boussinesq and hydrostatic approximations. The model also adopts a second order turbulent closure for coefficients of vertical viscosity and diffusion; Smagorinsky parameterization for horizontal viscosity and diffusion; leapfrog scheme for time and horizontal space integration (explicit scheme of 2nd order, centered in the time and space), and an implicit scheme for the vertical integration [19]. For the spatial differentiation, the model uses an alternating Arakawa C-type grid, suitable for high-resolution models (spacing less than 50 km).

The model was processed for 31 years (from 1979 to 2009) and the first year was discarded to avoid the influence of initial conditions at rest. The horizontal grid resolution was set to 0.5° in longitude and latitude, and vertical resolution of 22 sigma (σ) levels of varying thickness, with the first 8 levels corresponding to 10% of the total depth.

The tidal potential was included in all runs and the results of the model were filtered each time step, averaging 5 points in space and 3 levels in time, in order to eliminate noise. The boundary conditions for the currents were fixed as no-gradients and monthly climatological values of temperature and salinity were prescribed at the open limits of the grid. Harmonic constants of tidal components were given at double boundaries, so that the elevations were partially clamped to harmonic oscillations with restoration period equivalent to the baroclinic time step.

Table 1 gives some of the conditions used in the model processing and Table 2 informs the input data.

Model parameters	Values
Internal time step (integration)	1800 s (baroclinic)
External time step (integration)	30 s (barotropic)
Coefficient of relaxation to sea surface temperature climatology	100 W/m ² /K
Constant horizontal diffusivity (Smagorinsky)	0.08
Initial value of the Smagorinsky diffusion coefficient	100
Inverse diffusivity horizontal Prandtl number	1
Relaxation coefficient of TS model calculations to climatology (for all sigma levels)	10 ⁻³
Weight assigned to the central point in the process of spatial averages	0.8

Table 1: Initial parameters used in the model.

Input data	Source
Bathymetric data	General bathymetric Chart of the Oceans (GEBCO)
Forcing of mean sea level at the boundaries is inserted at intervals of 24 h, with corresponding climatological averages	Ocean Circulation and Climate Advanced Model (OCCAM)
Harmonic tidal constants at the open contours	Model TPX07.1-version utilizes mission data TOPEX / POSEIDON [20]
Temperature and salinity annual climatology (inserted at the initial time, at each grid point)	World Ocean Atlas in its 2008 version (WOA08)
Relaxation of model results to climatology	Climate Forecast System Reanalysis (CFSR) [21]
Boundary conditions for winds and surface fluxes of heat and salt (every 6 hours)	Reanalysis of atmospheric model of the NCEP/NCAR [22]

Table 2: Input data used in the model.

Model validation

An analysis of the deviations of the model results against measurements of PIRATA project was performed, based on Pereira and Harari [12] and others, considering temperature data (time series and profiles) from moored buoys in the period 1997-2009 [9]. The location of PIRATA buoys is given in Figure 2.

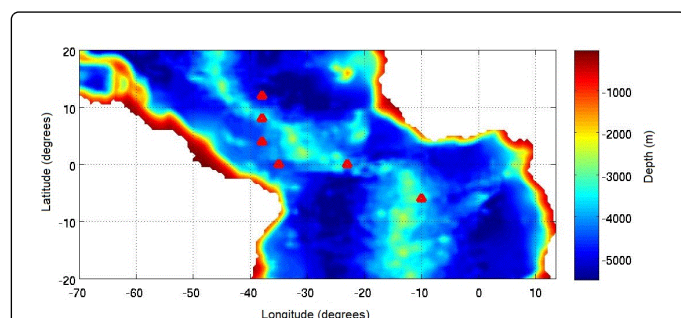


Figure 2: Location of PIRATA buoys with data used in the validation of the hydrodynamic model (red triangles) and bathymetry of the Tropical Atlantic region.

A second validation was performed, using surface temperature data from the Moderate Resolution Imaging Spectroradiometer (MODIS) sensor, with spatial resolution of 0.5 degrees in latitude and longitude, and temporal resolution of 8 days, being considered in this study the period 2003-2009. This data set was provided by Oregon State University (OSU) and is available in this site: <http://www.science.oregonstate.edu/ocean.productivity/>. In the comparison of the buoys data and model results, daily means were considered, while for MODIS data and model results, these were taken as 8 days means.

The model outputs and the buoys and MODIS data were displayed as time series, for each location or grid point, thus computing their mean values and standard deviations from the mean, for each variable, according to Vuolo [23]. For preventing errors due to outliers in time series, data differing from the mean more than three times the standard deviation were replaced by interpolated values (linear interpolations in time).

After editing the data, the method of least squares was applied to obtain trends and annual and semiannual signals of the series [24]. The

calculation of the correlation coefficient between pairs of series was done following Spiegel [25]. Apart from the coefficient of linear correlation, the following parameters were considered in the model validation:

The mean absolute error (1) where V_{mod} is the model result and V_{obs} is the observed value, being N the number of samples:

$$\theta = \frac{\sum (|V_{mod} - V_{obs}|)}{N} \quad (1)$$

The error relative to the mean (3), based on the average of observations (2):

$$\overline{V}_{obs} = \frac{\sum (|V_{obs}|)}{N} \quad (2)$$

$$\theta_r = \frac{\theta}{\overline{V}_{obs}} \quad (3)$$

This last value is sometimes multiplied by 100, giving the percentual error relative to the mean.

The Wilmott [6] parameter (4), where the value 1 represents a perfect fit between the results obtained by the model and the observations, while 0 represents a complete misfit:

$$WILM = 1 - \frac{\sum (|V_{mod} - V_{obs}|)^2}{\sum (|V_{mod} - \overline{V}_{obs}| + |V_{obs} - \overline{V}_{obs}|)^2} \quad (4)$$

Results and Discussion

Hydrodynamic model validation

Figure 3 has an example of the comparison PIRATA buoy x model results temperature series, above for the original series and below for the series after removal of the annual and semiannual signal, at 6°S 10°W. Figure 3 presents vertical profiles of temperature at 10°S 10°W, in January and July 2004. We observe very similar behavior of the collected data with the results obtained by the model with a slight underestimation of surface temperature and thermocline depth for the model.

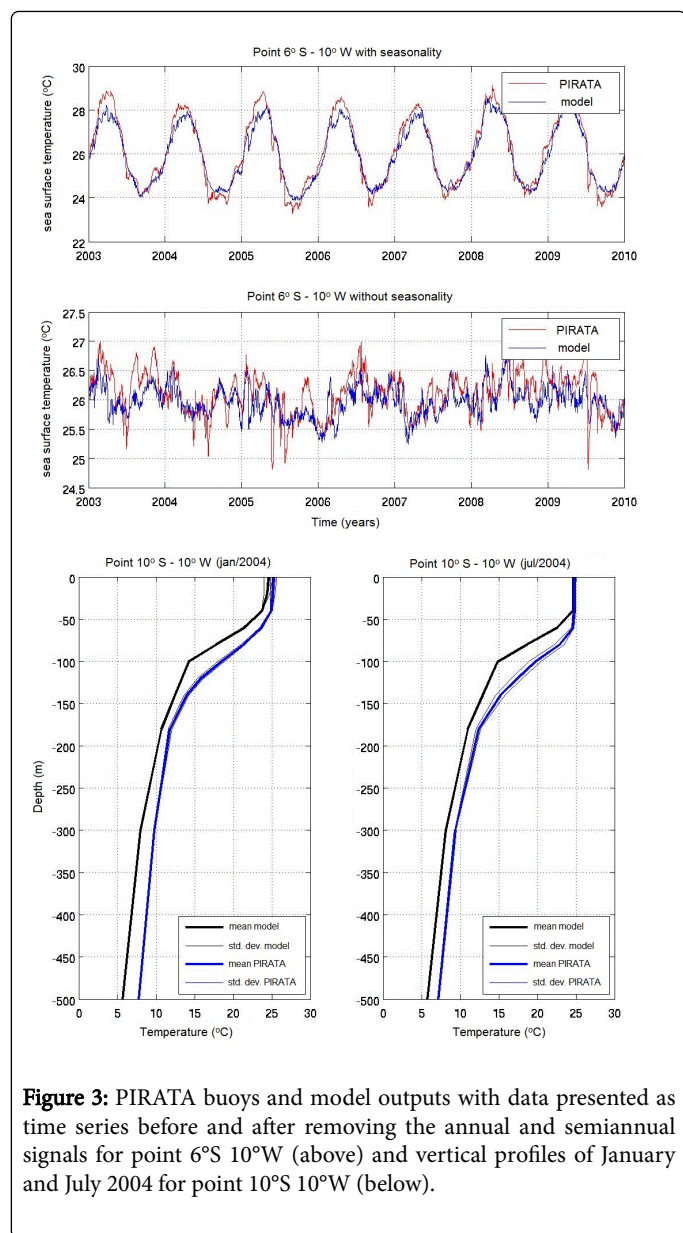


Figure 3: PIRATA buoys and model outputs with data presented as time series before and after removing the annual and semiannual signals for point 6°S 10°W (above) and vertical profiles of January and July 2004 for point 10°S 10°W (below).

Table 3 presents the comparative statistics between the buoys data and model outputs, considering the original series and the series after removal of the annual and semiannual signals. When keeping the seasonal signals, PIRATA data had an average value of $27.11 \pm 0.70^\circ\text{C}$, while the model had a mean of $26.55 \pm 0.78^\circ\text{C}$, with a mean difference of $0.56 \pm 0.44^\circ\text{C}$, which represents a slight underestimation of the temperatures calculated by the model to observations, a fact already observed visually. The biggest difference was at the point $0^\circ\text{N } 35^\circ\text{W}$, with 1.35°C , and the lowest point at $6^\circ\text{S } 10^\circ\text{W}$, with 0.15°C . Note that, in the model processing, at every time step there is a relaxation towards climatological values with a coefficient equal to 0.001, a value perhaps too high.

After removal of annual and semiannual signals, the time series have a lower average standard deviation, since a large amount of variability comes from the seasonality, but most of the difference is

within the deviation. When keeping the annual and semiannual signals, the linear correlation coefficients showed high values in the points analyzed ($\text{mean } 0.89 \pm 0.08$), while with the removal of these signals this coefficient reduces to an average value to 0.59 ± 0.07 . The Wilmott parameter, for the total series, also showed high values ($\text{mean } 0.83 \pm 0.18$), and after removal of seasonality this parameter has an average of 0.57 ± 0.15 .

Points (with seasonality)	0N23W	6S10W	8N38W	12N38W
Average PIRATA	26.59 ± 1.25°C	26.12 ± 1.60°C	27.71 ± 0.88°C	26.86 ± 1.15°C
Average model	25.82 ± 1.40°C	25.97 ± 1.35°C	27.37 ± 0.89°C	26.37 ± 1.15°C
Correlation coefficient	0.92	0.98	0.91	0.94
Wilmott parameter	0.88	0.98	0.92	0.93
Mean absolute error	0.81°C	0.34°C	0.42°C	0.53°C
Average relative error	3.04%	1.30%	1.52%	1.99%
Points (without seasonality)	0N23W	6S10W	8N38W	12N38W
Average PIRATA	26.59 ± 0.59°C	26.12 ± 0.37°C	27.71 ± 0.37°C	26.86 ± 0.45°C
Average model	25.82 ± 0.50°C	25.97 ± 0.26°C	27.37 ± 0.27°C	26.37 ± 0.30°C
Correlation coefficient	0.54	0.64	0.60	0.66
Wilmott parameter	0.54	0.74	0.63	0.61
Mean absolute error	0.80°C	0.26°C	0.39°C	0.51°C
Average relative error	3.02%	0.99%	1.39%	1.91%

Table 3: Comparative statistics of sea surface time series derived from the model and PIRATA measurements before and after the removal of annual and semiannual signals, at points $0^\circ\text{N } 23^\circ\text{W}$, $6^\circ\text{S } 10^\circ\text{W}$, $8^\circ\text{N } 38^\circ\text{W}$ and $12^\circ\text{N } 38^\circ\text{W}$.

There is no established reference value for the Wilmott parameter, but typical values around 0.5 indicate that the model reproduces about half of the observed variance [26]. Thus, it can be considered that values above 0.5 are significant, since most of the variance has been disregarded by the removal of annual and semiannual signals.

The mean absolute error with annual and semiannual signals had a mean value of $0.63 \pm 0.40^\circ\text{C}$ and an average relative error mean value of $2.34 \pm 0.01\%$. After removal of annual and semiannual signals, the errors had mean values of $0.61 \pm 0.40^\circ\text{C}$ and $2.21 \pm 0.02\%$. The comparative statistics of sea surface data from the buoys and model quantifies an error a little more than 0.5°C , so that, for more general analyzes, such as trends and large scale aspects, the model can be considered fully reliable.

When comparing the temperature profiles (Figure 3) similar patterns are again noticed, however, the model underestimation is greater in depth. The PIRATA profiles have average temperature of $19.25 \pm 1.51^\circ\text{C}$, while the model profiles have an average of $16.15 \pm 0.18^\circ\text{C}$, with a mean temperature difference of $3.09 \pm 1.58^\circ\text{C}$ (Table 4).

Points	8N38W-01/2004	8N38W-07/2004	10S10W-01/2004	10S10W-07/2004
Average PIRATA	18.04 ± 7.25°C	18.87 ± 7.81°C	17.98 ± 6.53°C	18.44 ± 6.61°C
Average model	16.13 ± 7.28°C	16.31 ± 7.59°C	16.02 ± 6.77°C	16.50 ± 6.92°C
Correlation coefficient	0.98	0.97	0.99	0.97
Wilmott parameter	1.00	0.99	0.99	1.00
Mean absolute error	0.08°C	0.36°C	0.34°C	0.08°C
Average relative error	0.59%	2.57%	2.67%	0.62%
Points	8N38W-01/2006	8N38W-07/2006	4N38W-01/2006	4N38W-07/2006
Average PIRATA	18.99 ± 7.42°C	19.66 ± 8.00°C	21.18 ± 8.04°C	21.81 ± 7.72°C
Average model	16.05 ± 7.34°C	16.20 ± 7.63°C	15.94 ± 8.17°C	16.07 ± 8.23°C
Correlation coefficient	0.98	0.94	0.85	0.83
Wilmott parameter	0.99	0.99	0.99	1.00
Mean absolute error	0.12°C	0.29°C	0.23°C	0.00°C
Average relative error	0.89%	2.02%	1.68%	0.02%

Table 4: Comparative statistics of temperature profiles derived from the model and PIRATA buoys, in the vertical profiles at 8°N 38°W and 10°S 10°W (in January and July 2004) and 8°N 38°W and 4°N 38°W (in January and July 2006).

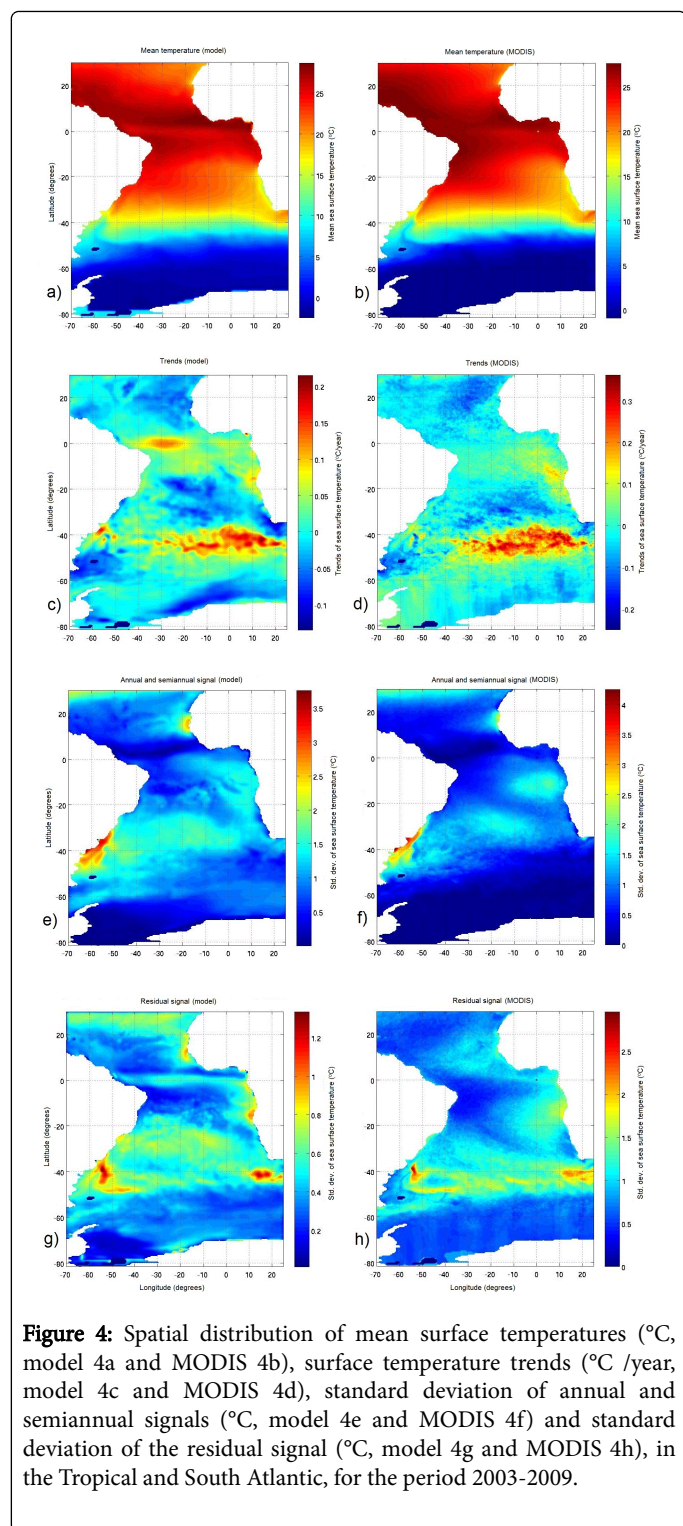
In the profiles comparison, the linear correlation coefficient and the Wilmott parameter showed high values, with respective averages of 0.94 ± 0.06 and 0.99 ± 0.00 . These values were expected, since they reflect the general behavior of the compared curves. The mean absolute error has average of $0.19 \pm 0.14^\circ\text{C}$ and the error on the average value is $1.38 \pm 0.99\%$, again relatively low values. In the case of the profiles comparison, the amount of points is very small, which affect the calculation.

In fact, there is an underestimation not only in the temperature profile as a whole, but the depth of the thermocline is also underestimated, with the model narrowing the mixed layer. The discrepancies in the thermocline depths are probably due to errors in the data fluxes of heat and salt specified as boundary conditions for the processings.

Continuing the model validation, sea surface temperature outputs were compared to MODIS measurements, for the entire area of interest, in the period 2003-2009 (Figure 4). Initially, we observe very similar patterns in the distribution of averages, with minor differences in some regions such as lower advection of colder waters north of the southern Brazilian coast, or less advection of warm waters in the region of the Agulhas Current Retroflexion (ACR), in the model calculations. Another difference is the occurrence of colder waters in the equatorial region by model calculations. This indicate an exaggeration of the modeled equatorial upwelling, which would explain the underestimation of the temperatures calculated by the model at points compared to PIRATA, which are close to this region.

Temperature distributions	MEAN	TREND	Standard dev. (annual and semi)	Standard deviation (residual)
Average MODIS	13.94 ± 11.09°C	$(0.11 \pm 7.20) \cdot 10^{-2}^\circ\text{C}/\text{year}$	0.69 ± 0.57°C	0.88 ± 0.33°C
Average model	14.18 ± 10.89°C	$(0.51 \pm 4.56) \cdot 10^{-2}^\circ\text{C}/\text{year}$	0.97 ± 0.49°C	0.45 ± 0.17°C
Correlation coefficient	0.99	0.77	0.84	0.60
Wilmott parameter	0.99	0.90	0.86	0.53
Mean absolute error	0.84°C	$(3.64) \cdot 10^{-2}^\circ\text{C}/\text{year}$	0.33°C	0.44°C
Average relative error	5.94%	70.59%	47.94%	49.63%

Table 5: Comparative statistics of the distributions of model outputs and MODIS observations, for temperature residuals (total minus annual and semiannual signals), for the study area, in the period 2003-2009.



The model had an average temperature of $14.18 \pm 10.89^{\circ}\text{C}$, while the satellite had mean $13.94 \pm 11.09^{\circ}\text{C}$ (Figure 4), with mean difference $-0.25 \pm 1.41^{\circ}\text{C}$, which shows a slight overestimation of the model to the sampled values (see statistics on Table 5). The linear correlation coefficient between these distributions was 0.99 and the Wilmott parameter 0.99, confirming the similarity of the distributions, as

observed visually. The mean absolute error is 0.84°C and the average relative error is almost 6%, again relatively low values.

The trends of temperatures computed by the model and measured by the satellite also are similar (Figure 4), but now the differences are more evident than for the distributions of the averages. The model showed a region at the Equator with strong positive trend ($0.2^{\circ}\text{C}/\text{year}$), which is not visible in the remote sensing data. The model also showed a strong trend (of the same order) of warming near the mouth of the La Plata River and further east up to 20°W , and cooling in the upper region of the South Atlantic Subtropical Gyre (SASG) and near the south coast of the African continent, while MODIS data have less intense trends.

The model showed an average trend of $(0.51 \pm 4.56) \cdot 10^{-2}^{\circ}\text{C}/\text{year}$, while the MODIS trend averaged $(0.11 \pm 7.20) \cdot 10^{-2}^{\circ}\text{C}/\text{year}$, with average difference between trends of $(-0.40 \pm 4.73) \cdot 10^{-2}^{\circ}\text{C}/\text{year}$, representing an average behavior for the whole region, the more intense positive trends calculated by the model, although the more intense extremes are found in MODIS data. These distributions present values of linear correlation coefficient of 0.77 and Wilmott parameter 0.90, values considered high, but lower than those shown in the comparison of the mean temperatures. The mean absolute error showed a value of $(3.64) \cdot 10^{-2}^{\circ}\text{C}/\text{year}$, and an average relative error of 70.59%, relatively high values.

Comparing the standard deviations of the annual and semiannual signals (Figure 4), distributions show great similarities, although there are some disparities, as the higher model values in the region north of the African coast. The model averaged the distribution of the parameter as $0.97 \pm 0.49^{\circ}\text{C}$, while the MODIS showed a mean of $0.69 \pm 0.57^{\circ}\text{C}$. The average of the differences between the distributions of the standard deviations was $-0.28 \pm 0.31^{\circ}\text{C}$, which demonstrates a general overestimation of the intensity of the signals by the model, although extreme values are larger in MODIS data set. The linear correlation coefficient of these distributions showed a value of 0.84 and the Wilmott parameter 0.86, both values considered high, reflecting the similarities found in the distribution patterns. The mean absolute error is 0.33°C and the average relative error 47.94%, due to some large differences in the values of the distributions.

Finally, the model and MODIS distributions of the standard deviations of the temperatures of the residual signal (after removal of annual and semiannual contributions) are similar, but with marked differences, such as higher values in the equatorial region and points of upwelling along the African coast presented by the model (Figure 4). The average presented by the model is $0.45 \pm 0.17^{\circ}\text{C}$, while the remote sensing had average of $0.88 \pm 0.33^{\circ}\text{C}$. The average difference between the distributions is $0.43 \pm 0.26^{\circ}\text{C}$, which shows smaller model variabilities. The linear correlation coefficient of these distributions was 0.60 and Wilmott parameter 0.53, values still above 0.5, but relatively low, demonstrating the discrepancies found in the distributions. The mean absolute error is 0.44°C and the average relative error 49.63%, due to discrepancies in the distributions.

Completing the comparative analysis, due to the high levels of linear correlation and Wilmott parameter found in the surface data, it could be considered that the results obtained by the model for the temperature at the surface are representative of the real ocean. The analysis in the equatorial region also pointed to the validity of such data, highlighting the occurrence of errors in depth. Moreover, other results of the implemented model, such as elevation fields and currents at the surface, have features and general distributions similar to those

established in the literature, for the region of interest, and these aspects are discussed in the following section. Therefore, it is valid to use the model for further analyzes and correlations, such as the ones with biotic observations, especially those of species that live near to the surface.

Distribution of physical variables

The horizontal distribution of the average surface temperature, trends and standard deviation (of seasonal and residual signals) were shown above, with respective statistical parameters (Figure 4 and Table 5). The distribution of the average temperature shows a temperature increase with decreasing latitude, with a steep gradient of around 40°S latitude, where the South Atlantic Current (SAC) flows. Other features at this latitude are the cold water intrusion (with deviation to the north of the isotherms) in the region of the Brazil-Malvinas Confluence (BMC) and intrusion of warm water (with deviation to the south of the isotherms) in the region of the ACR, and posterior transport for the Benguela Current [14]. This standard in the region of the Brazil-Malvinas Confluence (BMC) was verified by Teixeira et al. [27] in AVHRR/NOAA imaging (Advanced Very High Resolution Radiometer/NOAA) for the period from 1993 to 2001. Are visible, too, the effects caused by the SASG through the scattering of the isotherms to the north (cooler water) in the region of the Benguela Current and to the south (warmer water) in the region of the Brazil Current. The same behavior is seen to the north, in the southern part of the North Atlantic Subtropical Gyre (NASG).

In the distribution of standard deviations of temperature, it can be noted that the regions in which usually occur higher values are those that have high temperature gradients and occurrence of coastal upwelling. Concerning the standard deviation of the annual and semiannual signals, results a greater intensity in the Brazilian coast, near the area of BMC and in the upwelling region north of the African coast. The spatial variability of seasonality in surface temperature, the intertropical region, is verified by Hastenrath and Picaut [28,29]. Comparing seasonal with residual signals, the first presents higher values of standard deviations. By observing the standard deviation of the residual signal, the regions of equatorial upwelling, BMC and ACR are notable. The strongest annual and semiannual signals are verified by Teixeira et al. [27] in the region of BMC, confirming the spatial distribution pattern observed in this data.

The distribution of surface temperature trends, for the period studied, showed an average positive trend for the entire region. This shows an average increase in surface temperature for the period. This distribution pattern showed high positive values in the equatorial region and around the latitude 40°S (the region of highest temperature gradient). Negative trends were observed in the region south of the African continent, within the SASG, south of the American continent and around the Antarctic continent. These trends present, in the regions of extremes, values with the same order of magnitude as found in standard deviations, which indicate the importance of these values. This also indicates the importance of using longer time series to check a possible consolidation of these trends. An example of a similar study is that of Cheng and Qi [30], who computed trends of sea level variability in South China Sea with a 13 years altimetry record, and found opposite trend patterns, thus dividing the series into two periods, with distinct behaviors.

The temporal distribution of mean surface salinity (Figure 5) follows the pattern observed by Boyer and Levitus [31] in the annual average and standard deviation of WOA98 monthly averages. The distribution

at the surface here obtained showed a mean value of $35.14 \pm 1.99\text{‰}$, with a pattern resulting from the relationship between evaporation, precipitation and river flows, with low salinity at the mouth of major rivers (Congo, La Plata and Amazon) and upwelling off the Angolan coast and Argentina Platform. In these regions, there is a spread of low salinity that follows the pattern of the local currents, as the observed by Picaut [29]. In the region of the mouth of the La Plata River, the low salinity seems to spread out somewhat north (coast of Rio Grande do Sul), unlike the pattern found by Boyer and Levitus [31] who showed a greater spread north to the region of Cabo Frio (coast of Rio de Janeiro).

The trend of salinity distribution averaged $(0.02 \pm 2.24) \cdot 10^{-2}\text{‰/year}$. Greater positive values were detected in the regions of the mouth of the Amazon and Congo rivers and in the region of the Argentinian Continental Shelf. This indicates a trend of increasing salinity for the period. On the other hand, strong negative values are found at the mouth of the La Plata River and in the region south of the African continent, near latitude 40°S (Figure 5).

The standard deviation of salinity at the surface, after removal of annual and semiannual signals, averaged $0.18 \pm 0.16\text{‰}$ (Figure 5). The distribution pattern showed high values in regions of discharges of large rivers and coastal upwelling, and the occurrence of extremely low values in the southern portion of the African coast and low values in the contour that follows the SASG. The standard deviation of annual and semiannual signals showed a mean value of $0.15 \pm 0.14\text{‰}$ (Figure 5). This average is lower than that of the residual series, denoting high values, beside the regions already evidenced in the standard deviation of the series without seasonality, also around the vicinity of the Antarctic continent and within the subtropical gyre. It is remarkable a minimum deviation in the region of introduction of the Antarctic Circumpolar Current (ACC) in the South Atlantic.

The average surface elevations showed an average value of -0.56 ± 0.79 m (Figure 6). This distribution showed a specific pattern, with a triangular region of high positive values in the interior of the SASG, centered in the region of Rio Grande Rise. There is a strong gradient in the belt of latitude 45°S, with negative elevations in the polar region and a negative core south to the region of BMC. This standard of surface elevations was verified by Barron et al. [32].

The distribution of surface elevation trends has spatial average of $(-0.04 \pm 0.12) \cdot 10^{-2}$ m/year (Figure 6). Strong positive trends are found in the southern coast of the American continent, in the region between the Equator and 10°S and in the eastern portion of the belt between 40°S and 60°S. These trends have order of magnitude lower than the deviations, so they cannot be considered as conclusive.

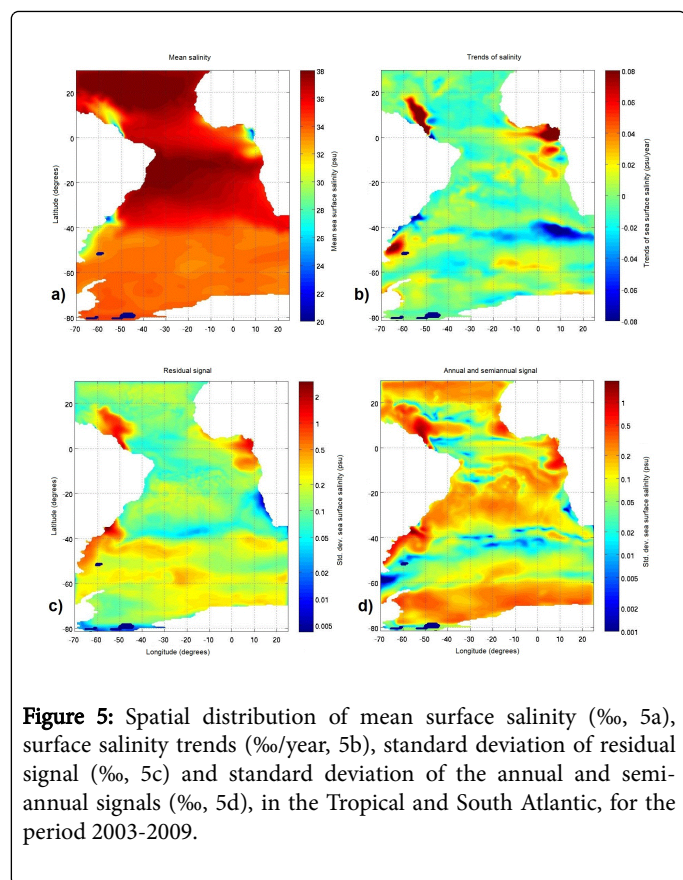


Figure 5: Spatial distribution of mean surface salinity (‰, 5a), surface salinity trends (‰/year, 5b), standard deviation of residual signal (‰, 5c) and standard deviation of the annual and semi-annual signals (‰, 5d), in the Tropical and South Atlantic, for the period 2003-2009.

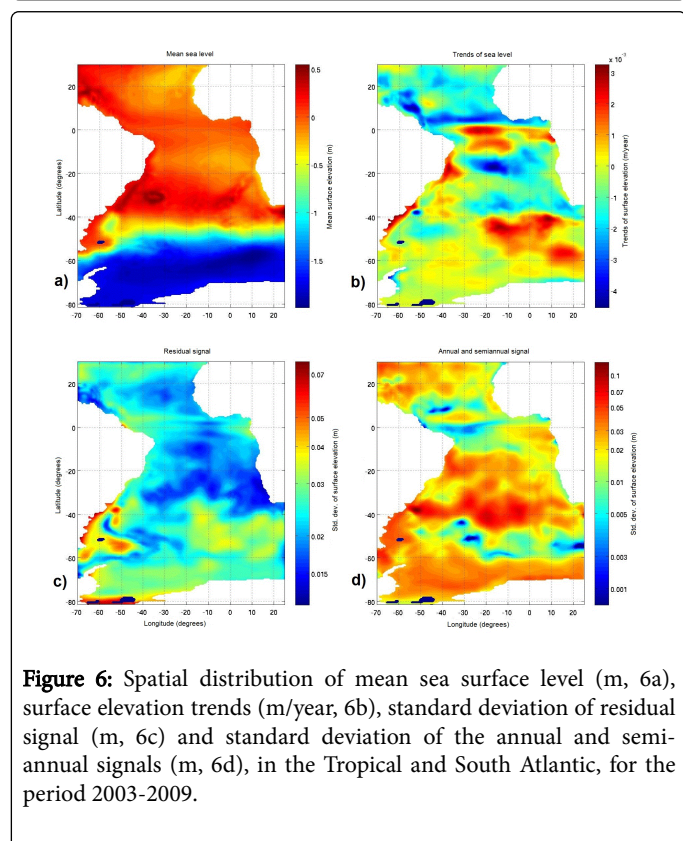


Figure 6: Spatial distribution of mean sea surface level (m, 6a), surface elevation trends (m/year, 6b), standard deviation of residual signal (m, 6c) and standard deviation of the annual and semi-annual signals (m, 6d), in the Tropical and South Atlantic, for the period 2003-2009.

The standard deviation after removal of annual and semiannual signals averaged 0.03 ± 0.01 m (Figure 6). Maximum values were found in the coastal region and adjacent to the southern extreme of the American continent, with lower values in the region north of latitude 40°S . The standard deviation of annual and semiannual signals averaged 0.02 ± 0.01 m (Figure 6), with a predominance of low values near the equatorial region and in the belt between 40°S and 60°S . The highest values were found in the area near the mouth of the La Plata River, spreading eastward around the same latitude. Schouten, Matano and Strub [33] found that, in the Equatorial Atlantic, the seasonal cycle is dominant in surface elevation data.

The distribution of the average intensities of surface currents (Figure 7) showed a mean value of 11.58 ± 12.01 cm/s. Maximum values were found in the equatorial region, the South Equatorial Current (SEC) and the north coast of South America, a region of the North Brazil Current (NBC). Note, too, the region of intense currents south of the American continent, from the Malvinas Current (MC) to the confluence with the Brazil Current, and the whole range between 40°S and 60°S , which comprises the SAC and the ACC. This distribution is observed for the Tropical Atlantic with data collected by drifters in different periods [34,35]. It is remarkable, too, the effect of bathymetric features in the currents, since the center of SASG, bypassing the Rio Grande Rise and meandering in the region of Walvis Ridge.

The distribution of the trends showed values of -0.02 ± 0.33 cm/s/year (Figure 7). It is remarkable the occurrence of strong negative trends in the region of the SEC and the NBC, denoting their intensity weakening. On the other hand, north and south SEC have strong positive trends, followed by a slight positive trend in the region of the MC.

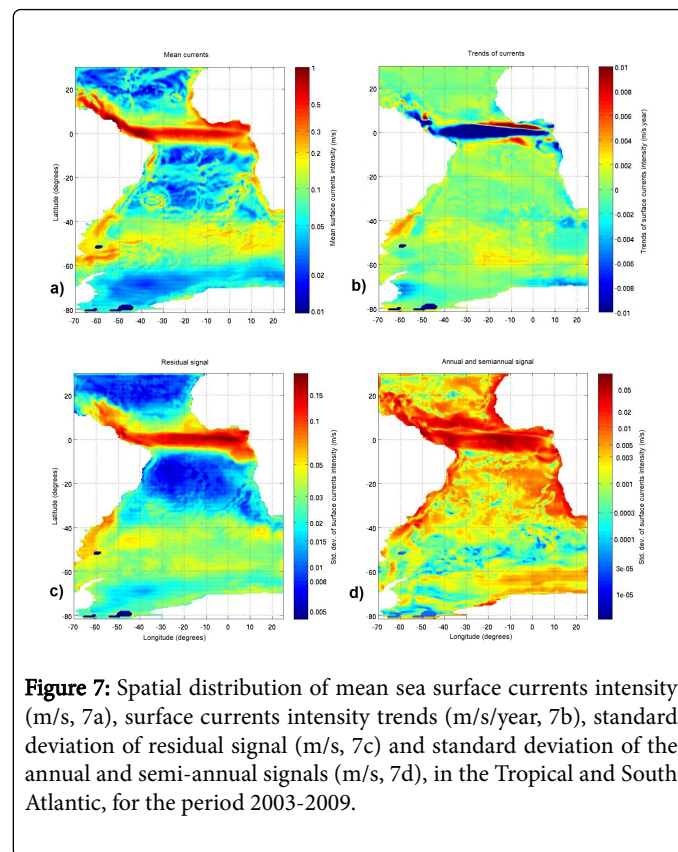


Figure 7: Spatial distribution of mean sea surface currents intensity (m/s, 7a), surface currents intensity trends (m/s/year, 7b), standard deviation of residual signal (m/s, 7c) and standard deviation of the annual and semi-annual signals (m/s, 7d), in the Tropical and South Atlantic, for the period 2003-2009.

The standard deviation after removal of annual and semiannual signals in the currents intensity has spatial average of 3.18 ± 2.67 cm/s. Its distribution follows very closely the pattern of distribution of the mean values, so that greater deviations occur in regions of greater currents intensity (Figure 7). The distribution of the standard deviation, referring to the annual and semiannual signals, showed an average of 0.57 ± 0.96 cm/s, a value much below the previous deviation (Figure 7). This indicates that the standard deviation of the currents intensity is not dominated by seasonality. It appears, also, a pattern of higher values in the region of the SEC and the NBC, but, in contrast to the residual signal, low values in the region of the ACC. This pattern for the annual and semiannual signals resembles those seen in the equatorial region by Lumpkin and Garzoli [34].

Conclusions

The results presented in the model validation and the comparisons with literature allow us to consider the model valid for more general analyzes, especially for large-scale processes near to surface. Some improvements are still needed in the model, particularly in regard to modeling the deep circulation.

The analysis of the distributions of means, trends and standard deviations, in the period from 2003 to 2009, demonstrates different patterns for each variable. Trend analyses identify interesting characteristics, as the extremely high trends of surface temperature found in the Equatorial region and in the latitude belt of 40°S, reaching +0.2°C/year. Was observed a trend of -0.01 m/s/year for the equatorial surface currents, surrounded by trends of +0.01 m/s/year off the African coast, at about 3°N and 3°S. However, is necessary a more detailed analysis in a longer period for more conclusive affirmations about these trends.

An analysis of the distributions of the standard deviations shows that seasonality is not always the main factor responsible for most of the standard deviations, such as for the intensity of the currents in the equatorial region.

References

- O'Brien JJ (1985) *Advanced Physical Oceanographic Numerical Modeling*. D Reidel Publishing Company. Dordrecht, p: 608.
- Blumberg AF, Mellor GL (1987) A description of a three-dimensional coastal ocean circulation model. *Three-Dimensional Coastal Ocean Models* 4: 1-16.
- Ezer T, Mellor GL (1994) Diagnostic and prognostic calculations of the North Atlantic circulation and sea level using a sigma coordinate ocean model. *J Geophys Res* 99: 159-171.
- Ezer T, Mellor GL (1997) Simulations of the Atlantic Ocean with a free surface sigma coordinate ocean model. *J Geophys Res* 102: 647-657.
- Ezer T, Mellor GL (2000) Sensitivity studies with the North Atlantic sigma coordinate Princeton Ocean Model. *Dynamics of Atmospheres and Oceans* 32: 185-208.
- Wilmott CJ (1981) On the validation of models. *Physical Geography* 2: 184-194.
- Lewis K, Allen JI (2009) Validation of a hydrodynamic-ecosystem model simulation with time-series data collected in the western English Channel. *J Mar Syst* 77: 296-311.
- Chu PC, Lu S, Chen Y (2001) Evaluation of the Princeton Ocean Model using the South China Sea Monsoon Experiment (SCSMEX) Data. *Atmos Oceanic Technol* 18: 1521-1539.
- Bourlès B, et al. (2008) The PIRATA Program: History, Accomplishments, and Future Directions. *Bull Am Meteorol Soc* 89: 1111-1125.
- Camargo R, Harari J (2001) Operational forecast of surges in the Southwestern Atlantic. *Proceedings of the 20th International Conference on Offshore Mechanics and Arctic Engineering - OMAE 2001 Rio de Janeiro, Brasil*, p: 5.
- Camargo R, Harari J, França CAS (2006) Downscaling the ocean circulation on Western South Atlantic: hindcasting, monitoring and forecasting purposes. *The 8th International Conference on Southern Hemisphere Meteorology and Oceanography, 8ICSHMO, Foz do Iguaçu, Brasil*, pp: 507-511.
- Pereira NES, Harari J (2010) Comparative study of meteorology, hydrodynamics and primary production in South and Tropical Atlantic Ocean through numerical modeling and remote sensing. *Resumos do III Congresso Brasileiro de Oceanografia CBO 2010. Rio Grande, RS* 1: 3971-3973.
- Cirano M, et al. (2006) The Oceanic circulation of large-scale in the South Atlantic region based on global circulation model OCCAM. *Rev Bras de Geof* 24: 209-230.
- Peterson RG, Stramma L (1991) Upper-level circulation in the South Atlantic Ocean. *Prog Oceanog* 26: 1-73.
- Gorgon AL, et al. (1989) Brazil-Malvinas Confluence-1984. *Deep Sea Res* 36: 359-384.
- Stramma L, Schott F (1999) The mean flow field of the tropical Atlantic Ocean. *Deep Sea Res II* 46: 279-303.
- Baptista MC (2000) An analysis of surface wind field over the ocean Tropical and South Atlantic using scatterometer data from ERS. *Masters Thesis, National Institute for Space Research, São José dos Campos*, p: 118.
- Harari J, Camargo R, França CAS (2005) Simulations and predictions of the tidal and general circulations in the South and Tropical Atlantic: high resolution grids in the Brazilian shelves. *Afro-America Gloss News, Revista do Global Sea Level Observing System (GLOSS), patrocinada pela Comissão Oceanográfica Intergovernamental (COI)* 9: 1-7.
- Harari J, Gordon M (2001) Numerical simulations of Substance Dispersion in Porto and Santos Bay, under the Tidal action and Winds. *Journal of Water Resources* 6: 115-131.
- Egbert GD, Bennett AF, Foreman MGG (1994) TOPEX/POSEIDON tides estimated using a global inverse model. *J Geophys Res* 99: 821-852.
- Saha S, et al. (2010) The NCEP Climate Forecast System Reanalysis. *Bull Amer Meteor Soc* 91: 1015-1057.
- Kalnay E (1996) The Ncep/Ncar 40-year reanalysis project. *Bull Am Meteorol Soc* 77: 437-470.
- Vuolo JH (1992) *Fundamentos da Teoria dos Erros*. 2nd edn. Sao Paulo: Editora Edgard Blücher LTDA, p: 249.
- Emery WJ, Thomson RE (2001) *Data Analysis Methods in Physical Oceanography*. 2nd edn. Elsevier Science Amsterdam. p: 658.
- Spiegel MR (1992) *Theory and Problems of Probability and Statistics*. 2nd edn. New York: McGraw Hill, p: 298.
- Hetland RD, Dimarco SF (2012) Skill assessment of a hydrodynamic model of circulation over the Texas-Louisiana continental shelf. *Ocean Modelling* 44: 64-76.
- Teixeira CEP, et al. (2009) On the temporal variability of the sea surface temperature in the Southwestern Atlantic based on the analysis of "Pathfinder AVHRR/NOAA" images. *Revista Brasileira de Cartografia* 61: 207-221.
- Hastenrath S (1984) Interannual Variability and Annual Cycle: Mechanisms of Circulation and Climate in the Tropical Atlantic Sector. *Mon Wea Rev* 112: 1097-1107.
- Picaut J (1983) Propagation of the seasonal upwelling in the eastern equatorial Atlantic. *J Phys Oceanogr* 13: 18-37.
- Cheng X, Qi Y (2007) Trends of sea level variations in the South China Sea from merged altimetry data. *Global and Planetary Change* 57: 371-382.
- Boyer TP, Levitus S (2002) Harmonic analysis of climatological sea surface salinity. *J Geophys Res* 107: 1-14.

-
32. Barron CN, et al. (2004) Sea Surface Height Predictions from the Global Navy Coastal Ocean Model during 1998-2001. *J Atmos Oceanic Technol* 21: 1876-1893.
 33. Schouten MS, Matano RP, Strub TP (2005) A description of the seasonal cycle of the equatorial Atlantic from altimeter data. *Deep-Sea Research I* 52: 477-493.
 34. Lumpkin R, Garzoli SL (2005) Near-surface circulation in the Tropical Atlantic Ocean. *Deep Sea Research I* 52: 495-518.
 35. Richardson PL, Philander SGH (1987) The Seasonal Variations of Surface Currents in the Tropical Atlantic Ocean: A Comparison of Ship Drift Data With Results From a General Circulation Model. *J Geophys Res* 92: 715-724.